Characterisation, conductivity and mechanical properties of the oxygen-ion conductor $La_{0.9}Sr_{0.1}Ga_{0.8}Mg_{0.2}O_{3-x}$

John Drennan,[a†] Viktor Zelizko,[a] David Hay,[a] Fabio T. Ciacchi,[a] S. Rajendran[b] and Sukhvinder P. S. Badwal*[b]

[a]*CSIRO, Division of Materials Science and Technology, Private Bag 33, Rosebank MDC, Clayton, Victoria 3169, Australia*

[b]*Ceramic Fuel Cells Limited, 710 Blackburn Road, Clayton, Victoria 3168, Australia*

The new oxygen-ion conductor $La_{0.9}Sr_{0.1}Ga_{0.8}Mg_{0.2}O_{3-x}$ has been prepared by conventional solid-state reaction at high temperatures and characterised by X-ray diffraction, scanning and transmission electron microscopy, and conductivity (four-probe dc and impedance) measurements. The room-temperature structure is orthorhombic, space group *Pnma* (no. 62), with $a=5.5391(7)$ Å, $b=7.8236(12)$ Å, $c=5.5224(7)$ Å. The material undergoes a phase transition at 445 K to a rhombohedral structure. Mechanical property measurements at room temperature and at 1173 K give average strength measurements of 162 ± 14 MPa and 55 ± 11 MPa respectively. Conductivity and ionic transport number measurements confirm predominantly ionic conduction. The contribution from the grain boundary conductivity is extremely small at temperatures below 673 K. At 1073 K, an ionic conductivity value of 0.12 S cm^{-1} was recorded in air.

It has been reported recently[1–4] that the $LaGaO_3$ perovskite substituted at the A and B sites shows good oxygen-ion conducting properties at elevated temperature. The most promising candidate materials have been shown to be those substituted at the A site with Sr and at the B site with Mg. The highest conductivity has been reported for the composition $La_{0.8}Sr_{0.2}Ga_{1-y}Mg_yO_{3-x}$ ($y=0.10$–0.15).[4] The electrolyte is commonly referred to as LSGM. The material is reported to be stable in both reducing and oxidising atmospheres up to 1223 K and shows a reported ionic conductivity of >0.1 S cm^{-1} at 1073 K and an ionic transport number of close to unity. Other materials with high ionic conductivity, such as doped ceria and bismuth oxide, are unstable in reducing environments and develop substantial electronic conductivity. The thermal expansion coefficient and the oxygen ionic conductivity domain (temperature and oxygen partial pressure range) are close to those of stabilised zirconias. The perovskite-based materials have often been discussed[5,6] as possible ionic conductors with the tantalising prospect of being able to engineer substitution of aliovalent cations onto both the A and B sites (ABO_3) with a view to introducing a variety of vacancy schemes and enhanced oxygen-ion conductivity. Until the recent report by Ishihara *et al.*[1] on LSGM, the results have been disappointing. With this discovery the renewed interest in this class of materials may prove to be a fruitful area of research.

Apart from ionic conductivity measurements and some information on the thermal expansion behaviour (thermal expansion coefficient $a=10^{-5}$ K^{-1} [3]) only limited physical property data are available for LSGM. Moreover, there is some confusion over the crystallographic characterisation of the material. In this paper we attempt to address these deficiencies by reporting mechanical property data, conductivity measurements (both four-probe dc and impedance) and crystallographic characterisation which was obtained using a combination of analytical electron microscopy and X-ray diffraction techniques.

Experimental

The powder of composition $La_{0.9}Sr_{0.1}Ga_{0.8}Mg_{0.2}O_{2.85}$ was prepared by conventional solid-state reaction at a high temperature. The required amounts of lanthanum oxide (>99%, calcined at 1000 °C for 2 h before use), gallium oxide (99.99%), magnesium oxycarbonate (>99%) and strontium carbonate (>99%) were mixed and milled together in isopropyl alcohol for 24 h followed by calcination at 1423 K for 4 h. The calcined powder was grey and X-ray diffraction pattern showed it to be single phase. The oxide powder was milled again in isopropyl alcohol for 24 h, dried and pressed into bar shapes for four-probe dc and impedance measurements, or disc shapes for mechanical strength measurements, and sintered at 1723 K for 15 h (heating and cooling rates of 300 °C h^{-1}). The sintered discs were darkish grey but had a density (6.58 g cm^{-3}) >98.5% of the theoretical.

The sintered and polished specimens were examined with a scanning electron microscope. Detailed characterisation of sintered samples was undertaken using a combination of analytical electron microscopy (ATEM) and X-ray diffraction techniques. ATEM was carried out on both crushed and ion beam thinned specimens using a Philips CM30 series electron microscope. Energy dispersive X-ray spectra were recorded using an EDAX 9900 system and all micrographs, diffraction patterns and spectra were recorded with the microscope operating at an accelerating voltage of 300 keV. In the case of the ion beam thinned specimens it was found necessary to coat the sample with a thin layer of carbon to avoid charging problems. A Siemens D500 diffractometer was used to collect X-ray diffraction patterns using graphite-monochromated Cu-Ka radiation. XRD data were also collected at 483 K using a locally constructed temperature stage for the D500 diffractometer. Refinement of structural parameters was carried out by Rietveld methods using the program WYRIET 3.[7]

Differential thermal analysis (DTA) measurements were made with a Stanton Redcroft Thermochemical Analyser TMA series 793. The heating rate used was 10 °C min^{-1}.

Four-probe dc conductivity measurements were performed in air as a function of temperature (673–1273 K) at 10–25 K intervals during both heating and cooling cycles and as a function of time at 1123 and 1273 K on different specimens. The specimens were *ca.* 20–22 mm long with linear conduction areas of *ca.* 0.21 cm^2. The details of the experimental set-up have been described in a previous publication.[8] For impedance measurements, specimens were cut from bars and had dimensions of $a=5.3$ mm, $b=7.5$ mm and thickness $t=3.9$ mm.

† Present Address: Centre for Microscopy and Microanalysis, The University of Queensland, Brisbane, QLD 4072, Australia.

Table 1 Room-temperature strength of LSGM samples[a]

sample	t^b/mm	w[c]/mm	load/N	strength/MPa
1	1.484	16.32	279	138
2	1.510	16.31	339	162
3	1.495	16.31	335	164
4	1.263	15.60	265	183
5	1.248	15.61	233	165
6	1.257	15.64	228	159

[a]Average strength = 162 ± 14 MPa. [b]t = thickness. [c]w = diameter.

Table 2 High-temperature strength of LSGM samples[a]

sample	t/mm	w/mm	load/N	strength/MPa
1	1.478	15.13	137	67
2	1.513	14.98	125	58
3	1.496	14.97	126	60
4	1.548	14.98	112	50
5	1.540	15.06	143	64
6	1.471	15.02	72	35
7	1.484	15.00	104	50

[a]Average strength = 55 ± 11 MPa at 1173 K.

Platinum paste electrodes sandwiched between platinum mesh were used for current collection. Impedance measurements were performed over the temperature range 573–723 K and the frequency range 5 Hz–5 MHz (with a Hewlett Packard 4192A impedance analyser) in air at 25 K intervals.

Transport number was measured by constructing a galvanic cell with platinum paste electrodes and exposing one side of the cell to air and the other side to controlled H_2–H_2O gas mixtures at different temperatures.

Flexural strength measurements were made at room temperature and at 1173 K. Disc-shaped sintered specimens (dimensions are presented in Tables 1 and 2) were used. Prior to testing, both surfaces of the discs were ground using a diamond wheel and one of the surfaces was polished to a 1 μm finish using diamond paste. This is to ensure that the tensile surface is free from any pre-existing flaws. The loading configuration for the test was similar to that described in the ASTM F394-78 [9] publication. In the room-temperature case, the three support balls were equally spaced on a circle of 12.098 mm diameter with the loading ram of 3.946 mm diameter. At 1173 K, support pins with hemispherical ends and having diameters of 3 mm were used. The pins were spaced equally on a circle of diameter 11.493 mm and the loading ram was 3.95 mm in diameter.

Results and Discussion

The material was easily fabricated into dense bodies. The microstructure of a polished and etched specimen is shown in Fig. 1. In general, very few but uniformly distributed pores were observed in the microstructure. Clearly a bimodal grain size distribution was observed in the microstructure. Small grains were in the 3–5 μm and large grains in the 15–25 μm size range. The room-temperature X-ray diffraction patterns of the prepared samples used in this study showed a basic perovskite-related structure. However, on closer examination it is clear that some reflections showed shoulders and splitting representing a reduction in symmetry. Goodenough and Feng[3] reported that the $La_{0.9}Sr_{0.1}Ga_{0.8}Mg_{0.2}O_{2.85}$ phase was cubic perovskite, whilst Ishihara *et al.*[1] have reported an orthorhombic structure for this material. In this study the powder patterns were indexed using the orthorhombic cell and Rietveld refinements carried out on this basis. The results of Rietveld full pattern refinement are shown in Fig. 2. The atomic model which gave the best fit to the data was orthorhombic, space group *Pnma* (no. 62), with refined cell dimensions $a = 5.5391(7)$ Å, $b = 7.8236(12)$ Å and $c = 5.5224(7)$ Å. Refinement converged to Bragg $R = 5.1\%$. Refined atomic coordinates are given in Table 3.

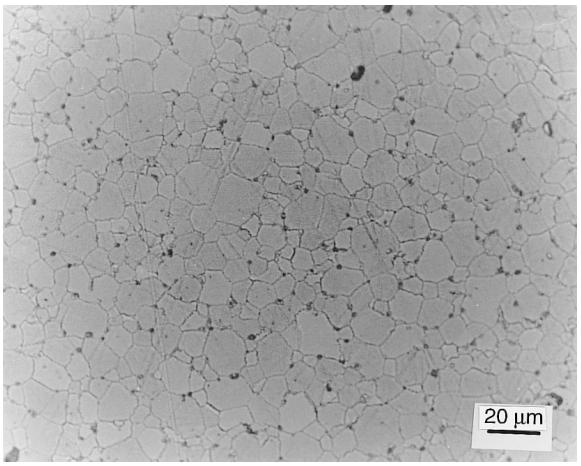

Fig. 1 Optical micrograph of an LSGM sample

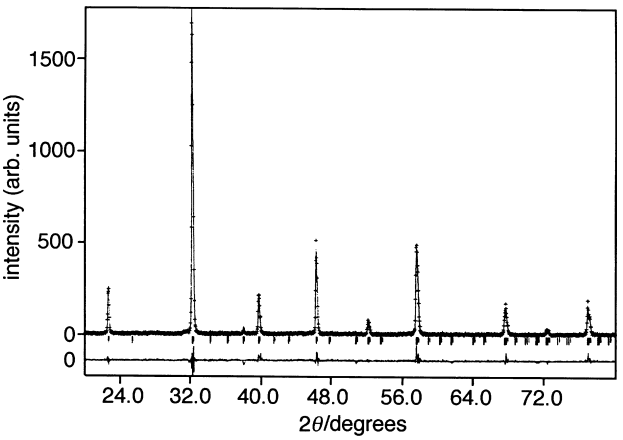

Fig. 2 Rietveld pattern refinement of LSGM as the orthorhombic (*Pnma*) structure. The observed XRD trace is shown, together with the theoretical trace using refined parameters, and a difference trace is shown below. Expected peak positions from the model structure are shown as bars.

The room-temperature symmetry was further confirmed by analytical transmission electron microscopy (ATEM). Convergent-beam electron diffraction patterns recorded from individual grains of the LSGM showed extra reflections which are not consistent with a primitive cubic cell. Fig. 3 shows an indexed orthorhombic pattern ([100]) based on the unit cell described above. To further confirm that the material was in fact homogeneous, energy dispersive X-ray spectra were recorded from a number of grains and an example is shown in Fig. 4. Clearly a solid-state reaction has taken place and La, Sr, Ga and Mg were detected; composition variations between grains were insignificant. Quantitative analysis determined using the peak intensities gave values close to the nominal composition but difficulties with overlapping peaks

Table 3 Refined fractional atomic coordinates with estimated standard deviations in parentheses

atom	$10^3x/a$	$10^3y/b$	$10^3z/c$
La	9998(14)	2500	−18(36)
Sr	9998(14)	2500	−18(36)
Ga	0	0	5000
Mg	0	0	5000
O1	4380(119)	2500	584(129)
O2	2409(127)	504(32)	7522(174)

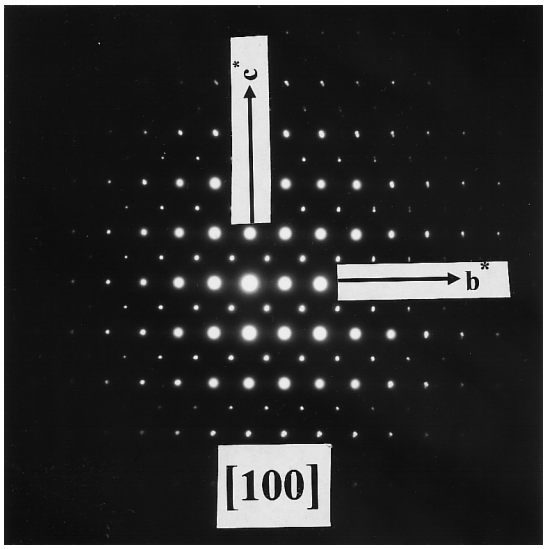

Fig. 3 The [100] diffraction pattern of an LSGM specimen

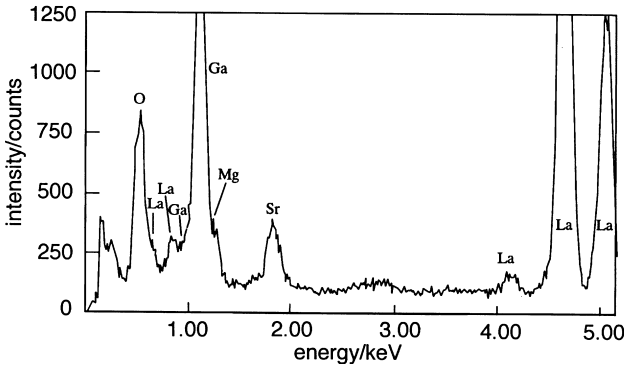

Fig. 4 A portion of the energy dispersive X-ray spectrum showing the presence of La, Sr, Ga and Mg in the grain of an LSGM specimen

and absorption effects introduced some uncertainties into these calculations.

A further observation of the microscopy revealed that the grains of LSGM at room temperature contained contrast features consistent with twinning. Microdiffraction patterns confirmed that these domains are associated with twinning and this is illustrated in Fig. 5. This phenomenon has been observed in electron microscopy studies of the related perovskite $LaGaO_3$.[10] It should be noted that extensive crystallographic studies have been made of $LaGaO_3$ and the material has an orthorhombic structure at room temperature with lattice parameters $a=5.5232(5)$ Å, $b=7.776(2)$ Å, $c=5.4925(7)$ Å and the space group *Pnma* (no. 62) satisfies the diffraction evidence. In addition, $LaGaO_3$ is known[11] to undergo a phase transition at 418 K in which the system transforms from orthorhombic symmetry to rhombohedral symmetry and the consequent readjustment gives rise to elimination of twins. DTA results obtained from the LSGM specimens examined in this work revealed that an endothermic peak was detected at 445 K, slightly higher than that reported for pure $LaGaO_3$ (418 K), but certainly indicating a phase transition. It is a logical assumption, therefore, that the twin boundaries observed in LSGM are a result of a possible phase transition similar to that observed in $LaGaO_3$. To further confirm the DTA results, high-temperature X-ray diffraction was employed to examine for any evidence of this phase transition. Indeed, evidence of a phase change is seen in the XRD data at 483 K. The group of peaks at 2h # 32° is seen as a doublet in the orthorhombic (*Pnma*) room-temperature structure. However, further splitting of this group of peaks is seen

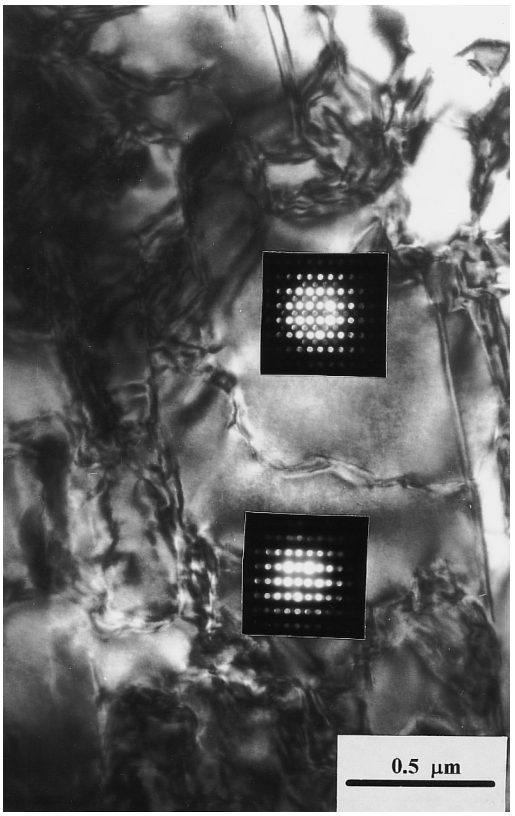

Fig. 5 Bright-field micrograph recorded from part of a grain of LSGM showing the strain and massive twinning which is a feature of this material. Inset in the micrograph are microdiffraction patterns recorded from the regions directly underneath the patterns. Clearly a twin relationship exists.

in the high-temperature trace, part of which is shown in Fig. 6, where peaks appear as a multiplet. This is characteristic of a change to rhombohedral (*R*3*c*) symmetry, where these peaks appear as a triplet, as observed for the phase transition at 418 K in $LaGaO_3$.[12] It should be noted that Petric *et al.*[4] observed extra reflections for LSGM in the electron diffraction pattern. They described these reflections as superstructure reflections resulting from the formation of microdomains. In the work reported in this study, although such reflections were observed, these could be fully indexed using the orthorhombic cell structure.

The consequence that this phase transition has on the suitability of LSGM as an electrolyte material is unknown but the amount of strain evident in the micrographs (Fig. 5)

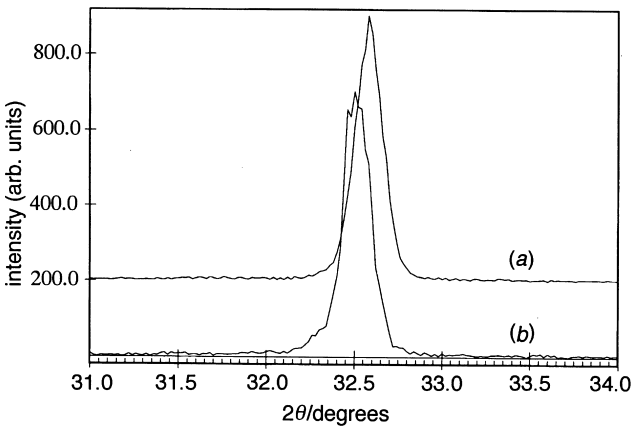

Fig. 6 Expansion of the peak structure near 32° showing the room-temperature (*a*) and 483 K (*b*) XRD traces

suggests that thermal cycling through the transition point may be deleterious to mechanical properties.

The results of strength measurements on LSGM samples at room temperature and at 1173 K are presented in Tables 1 and 2. The average strength determined was 162 ± 14 MPa at room temperature. Specimens dimensions, fracture loads and determined strength for 1173 K strength tests are given in Table 2. At this temperature the average strength determined for LSGM was 55 ± 11 MPa. The flexural strength of these materials is significantly lower in comparison to the zirconia-based electrolytes presently in use. It is worth mentioning here that the mechanical strength of fully stabilised zirconia is in the vicinity of 300 MPa at room temperature and 120 MPa at 1273 K.[13] For yttria–tetragonal zirconia ceramics, flexural strengths of around 1000 MPa and 350–400 MPa have been measured at room temperature and 1273 K respectively.[13]

Fig. 7 shows Arrhenius plots for the conductivity data of LSGM, 9 mol% Sc_2O_3–ZrO_2 and 9 mol% Y_2O_3–ZrO_2. Clearly the conductivity of LSGM is higher than that of 9 mol% Y_2O_3–ZrO_2, but over the temperature range 1073–1273 K the ionic conductivity values for both materials are comparable. Table 4 gives ionic conductivity values for several high-conductivity electrolyte materials. At 1073 K, the ionic conductivity of Sm_2O_3-doped ceria is slightly lower than that of LSGM. The activation energy values for conduction are given in Table 5. At high temperatures (1123–1273 K), the activation energy for LSGM was lower than for both 9 mol% Sc_2O_3–ZrO_2 and 9 mol% Y_2O_3–ZrO_2 materials.

Conductivity data as a function of time at 1123 and 1273 K for LSGM are displayed in Fig. 8. Only a slight decrease in the conductivity was observed with time at 1273 K. At 1123 K, the effect of time on conductivity was insignificant. This absence of any ageing process clearly indicates that the phase assemblage or the structure of the material is stable. This was further confirmed by transmission electron microscopy of the annealed (1273 K, 5000 min) specimen.

Impedance measurements on LSGM specimens over the 573–723 K range show a very low contribution from the grain boundary resistivity (Fig. 9). A slight decrease in the volume resistivity as a result of annealing at 1273 K could not be explained by the conductivity or activation energy data or by the detailed microstructural analysis.

In order to determine ionic transport number, small fuel cells were constructed with Pt air and fuel electrodes and LSGM as the electrolyte. Fig. 10 shows the results of open circuit voltage measurements at several temperatures for air *vs.* H_2–H_2O mixture. In all cases the measured voltage was close to the theoretical (ionic transport number close to unity) indicating that the material is mainly an ionic conductor.

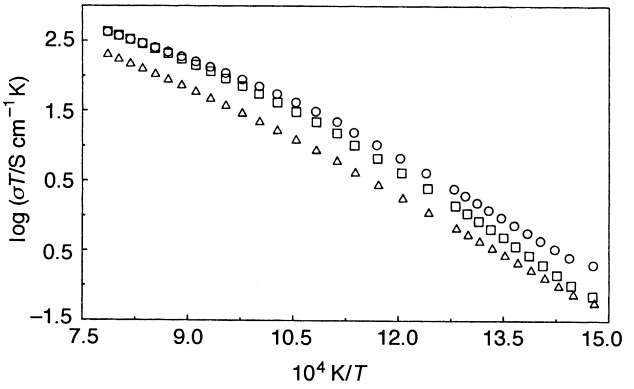

Fig. 7 Arrhenius plots (four-probe dc data) for LSGM (#), 9 mol% Sc_2O_3–ZrO_2 (%) and 9 mol% Y_2O_3–ZrO_2 (')

Table 4 Conductivity data for some high-conductivity oxygen-ion conducting electrolytes

system	s/S cm^{-1} (1073 K)	s/S cm^{-1} (1273 K)	ref.
LSGM	0.121	0.316	
$(ZrO_2)_{0.91}(Y_2O_3)_{0.09}$	0.046	0.166	14
$(ZrO_2)_{0.91}(Sc_2O_3)_{0.09}$	0.109	0.306	14
$(CeO_2)_{0.82}(Gd_2O_3)_{0.18}$	—	0.235	15
$(CeO_2)_{0.80}(SmO_{1.5})_{0.20}$	0.096	0.25	16
$(Bi_2O_3)_{0.80}(Er_2O_3)_{0.20}$	0.37[a]	—	17
$(Bi_2O_3)_{0.80}(Nb_2O_5)_{0.20}$	0.19[a]	—	18

[a]At 973 K.

Table 5 Activation energy data for LSGM, 9 mol% Sc_2O_3–ZrO_2 and 9 mol% Y_2O_3-ZrO_2

(*a*) From four-probe dc conductivity data:

	E_a/kJ mol^{-1}	
	400–450 °C	850–1000 °C
$La_{0.9}Sr_{0.1}Ga_{0.8}Mg_{0.2}O_{3-x}$	109 ± 3	64 ± 2
9 mol% Sc_2O_3–ZrO_2	130 ± 2	72 ± 3
9 mol% Y_2O_3–ZrO_2	107 ± 2	81 ± 3

(*b*) From impedance data[a] (300–450 °C):

	E_a/kJ mol^{-1}		
$La_{0.9}Sr_{0.1}Ga_{0.8}Mg_{0.2}O_{3-y}$	R_v	R_{gb}	R_{total}
before annealing	107 ± 1	97 ± 2	105 ± 1
after 1000 °C anneal, 5000 min	105 ± 1	96 ± 2	104 ± 1
after 850 °C anneal, 5000 min	106 ± 1	98 ± 2	105 ± 1

[a]R_v = volume (or lattice) resistivity, R_{gb} = grain boundary resistivity, $R_{total} = R_v + R_{gb}$.

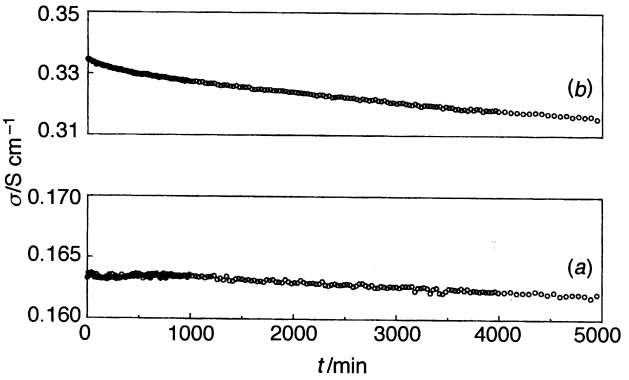

Fig. 8 Dc conductivity for LSGM as a function of time at 1123 (*a*) and 1273 K (*b*)

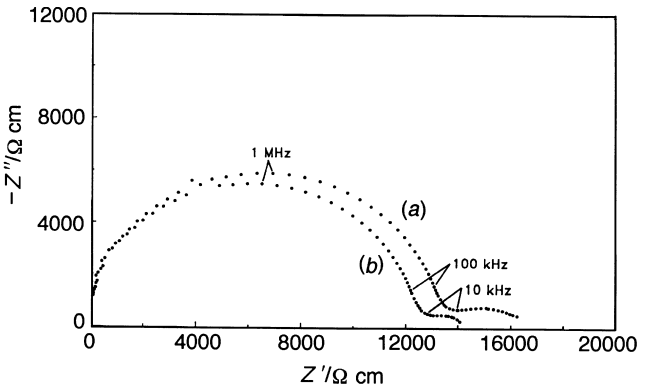

Fig. 9 Impedance plots at 623 K in air for LSGM before (*a*) and after (*b*) annealing at 1273 K for 5000 min

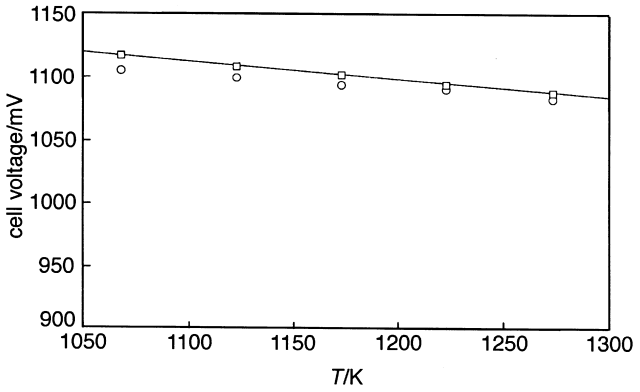

Fig. 10 Open-circuit voltage [measured (#), calculated (%)] for Pt, air|LSGM|Pt, H_2–2%H_2O cell as a function of time. The solid line represents the calculated cell voltage.

Conclusions

At 1273 K, the ionic conductivity of $La_{0.9}Sr_{0.1}Ga_{0.8}Mg_{0.2}O_{3-x}$ is higher by a factor of two compared to ZrO_2 doped with 8 mol% Y_2O_3; however, it was similar to that of ZrO_2 doped with 9 mol% Sc_2O_3. The major drawback of these materials as potential electrolytes for use in solid oxide fuel cells or other similar applications is the high cost of gallium compounds, related to its scarcity, and the low mechanical strength of LSGM, especially at the fuel cell operating temperatures. It is unlikely that such materials can be used in electrolyte-supported designs for solid oxide fuel cells or in applications where they must play some role in the structural design of a device. A more likely application would be in their use as thin coatings on an electrode substrate. Alternatively these materials may find use in sensors where the current-carrying capacity of the device is not important and the materials are used in small quantities.

The authors are thankful to Dr. S. P. Jiang for determining the ionic transport number, Miss Kristine Giampietro for specimen preparation and to Dr. K. Foger for reviewing this manuscript.

References

1 T. Ishhihara, H. Matsuda and Y. Takita, *J. Am. Chem. Soc.*, 1994, **116**, 3801.
2 T. Ishihara, H. Matsuda and Y. Takita, *Solid State Ionics*, 1995, **79**, 147.
3 M. Feng and J. B. Goodenough, *Eur. J. Solid State Inorg. Chem.*, 1994, **31**, 663.
4 A. Petric, P. Huang and A. Skowron, *Proc. 2nd Eur. SOFC Forum*, ed. B. Thorstensen, Druckerei J Kinzel, Göttingen, Germany, 1996, pp. 751–760.
5 J. B. Goodenough, A. Manthiram and J-F. Kuo, *Mater. Chem. Phys.*, 1993, **35**, 221.
6 A. F. Sammells, R. L. Cook, J. H. White, J. J. Osborne and R. C. MacDuff, *Solid State Ionics*, 1992, **52**, 111.
7 M. Schneider, Program WYRIET 3, version 3, D-8134 Pocking, West Germany, 1992.
8 S. P. S. Badwal, F. T. Ciacchi and D. V. Ho, *J. Appl. Electrochem.*, 1991, **21**, 721.
9 ASTM Designation: F 394–78.
10 M. Sundberg, P-E. Werner, M. Westdahl and K. Mazur, *Mater. Sci. Forum*, 1994, **166–169**, 795.
11 H. M. O'Bryan, P. K. Gallagher, G. W. Berkstresser and C. D. Brandle, *J. Mater. Res.*, 1990, **5**, 183.
12 Y. Wang, X. Liu, G.-D. Yao, R. C. Lieberman and M. Dudley, *Mater. Sci. Eng.* A, 1991, **132**, 13.
13 V. Zelizko, unpublished work.
14 S. P. S. Badwal, F. T. Ciacchi, J. Drennan and S. Rajendran, to be published.
15 T. Kudo and H. Obayashi, *J. Electrochem. Soc.*, 1976, **123**, 415.
16 K. Eguchi, T. Setoguchi, T. Inoue and H. Arai, *Solid State Ionics*, 1992, **52**, 165.
17 M. J. Verkerk, K. Keizer and A. J. Burggraaf, *J. Appl. Electrochem.*, 1980, **10**, 81.
18 T. Takahashi, H. Iwahara and T. Esaka, *J. Electrochem. Soc.*, 1977, **124**, 1563.

Paper 6/04563D; *Received* 1*st July*, 1996